Journal of The Electrochemical Society, **152** (9) B376-B387 (2005)
0013-4651/2005/152(9)/B376/12/$7.00 © The Electrochemical Society, Inc.

Inhibition of the Oxygen Reduction Reaction on Copper with Cobalt, Cerium, and Molybdate Ions

F. J. Presuel-Moreno,* M. A. Jakab,* and J. R. Scully**

Department of Materials Science and Engineering, University of Virginia, Charlottesville, Virginia 22904, USA

The inhibition of the oxygen reduction reaction (ORR) on copper was investigated after pretreatment with Co, Ce, and Mo ions at applied potential simulating galvanic coupling to AA2024-T3. Specifically, the effect of Ce(III), Co(II), and MoO_4^{2-} pretreatments on ORR was investigated in the mixed charge transfer, mass transport regime in pH 7-11 solutions using the Koutecky-Levich approach. Co reduces the ORR rate the most in more alkaline solutions (pH 9.5) while the Ce pretreatment works best in slightly less alkaline solutions (pH 7-8.2). Mo pretreatment was also most effective at pH 8.2 and was ineffective at pH 11. These results were consistent with chemical precipitation of $Co(OH)_2$ and $Ce(OH)_3$ or CeO_2. MoO_2 was rationalized to be formed by electrochemical reduction of MoO_4^{2-} on copper. This process was not operative at highly alkaline pH at applied potentials near the open circuit potential of AA2024-T3.
 [DOI: 10.1149/1.1997165]

Manuscript submitted September 28, 2004; revised manuscript received April 13, 2005. Available electronically August 8, 2005.

Corrosion usually proceeds on aluminum alloy 2024-T3 because of galvanic coupling between the anodic sites and intermetallic compounds which serve as cathodic sites. Oxygen reduction reaction (ORR) takes place at the Cu rich intermetallics or at areas where Cu is replated on the surface due to corrosion.[1-7] In contrast, corrosion is very slow on high-purity Al over a broad range of pH,[4,8] as the insulating Al-rich oxide significantly reduces the rate of ORR. However, Cu is a desired alloy addition to produce high strength Al alloys. Therefore, it is of interest to investigate the kinetics of ORR on Cu and the effect of some recently identified environmentally friendly inhibitors on the ORR.[a]

Traditionally, several methods have been used to protect aluminum alloys against corrosion (e.g., anodizing,[17] chromate conversion coating,[18] metallic cladding with Alclad,[19] corrosion protection compounds,[20] and solution phase inhibitors[21,22]). Chromate conversion coating (CCC) is the method used most often to protect aluminum alloys. CCC is widely used because it is a multifunctional inhibitor with an active corrosion inhibition property.[23-25] It can provide protection to distant sites and release can be triggered by alkaline hydrolysis.[26] However, Cr(VI) is toxic and carcinogenic. Health and environmental hazard considerations have motivated the interest to find replacements that are environmentally acceptable.

Recently, a new family of Al-Co-Ce-(Mo) alloys has been synthesized.[27] These alloys contain up to 10 atom % Co and Ce and are produced as amorphous glasses or nanocrystalline structures. Their excellent intrinsic corrosion resistance compared to conventional aluminum alloys[28] have been demonstrated. These Al-Co-Ce-(Mo) alloys could serve as multipurpose metallic coatings, acting as a protective layer, sacrificial anode, and as a source of active inhibitor. These alloys release Co^{2+}, Ce^{3+}, or MoO_4^{2-} ions depending on the acidity or alkalinity of the environment. Therefore, it is of interest to investigate specifically the effect of Co^{2+}, Ce^{3+}, or MoO_4^{2-} ions on ORR of Cu. Cu electrodes exposed to solutions containing the ions of interest (Co^{2+}, Ce^{3+}, or MoO_4^{2-}) are investigated in this study. These ions have been investigated to different degrees earlier,[23,25,29-67] but their effect on ORR of Cu is still not completely understood, in part because there is the need to separate and distinguish the effects of all inhibitors on both charge-transfer and mass-transfer controlled aspects of the ORR. Moreover, there could be added insight gained by fixing the near-surface pH with a buffered solution and systematically varying pH instead of allowing it to drift with applied potential, current, and time.

Preliminary results on the performance of Na_2MoO_4 appeared as early as 1979[37] in cooling water systems applications to protect Cu, Fe, and brass; Na_2MoO_4 was used with other inhibitors. Several studies of Mo in Al or Al alloys have been conducted.[32-37] Unfortunately, due to the low solubility of Mo in aluminum, conventional alloying techniques cannot be used.[68,69] Alternative procedures have been used to alloy Al with Mo, where a protective film is formed[70-72] that contains Mo oxides. Immersion in acidic solutions containing molybdate ion[32-34] and surface modification[35,36] are some examples of other methods used to integrate Mo in a protective film over aluminum alloys. The film formed after Mo treatment on aluminum has been reported to contain both Mo^{4+} and Mo^{6+}.[32] Molybdate ion has been mainly thought to be an anodic inhibitor[32-41] and little is known about its ability to act as a cathodic inhibitor. The anodic inhibiting effect of molybdate ions might be due to the reduction of Mo^{6+} to Mo^{4+} during film formation.[34] In summary, the role of MoO_4^{2-} as a cathodic inhibitor is not understood, but is intriguing because of the solubility of MoO_4^{2-} at high pH and its ability to be reduced from a soluble +6 oxidation state (MoO_4^{2-}) to an insoluble +4 oxidation state (MoO_2) at intermediate pH values.[73]

Cerium salts are nontoxic and, therefore, attractive as possible chromate replacements. Ce^{3+} cations can inhibit ORR at cathodes on aluminum alloys.[22,42] Ce^{3+} ions have been used alone, in combination with MoO_4^{2-} in an anodizing process,[35,36] or combined with other compounds.[29,43-45] Usually, $CeCl_3$ was the salt reported to be used.[22,42,46-48] The Ce^{3+} ion was found to inhibit the ORR on AA7075.[22,42] It has also been shown[53] that a Ce coating could have performance comparable to that of the chromate conversion coatings, but required a long time (4-5 days) to form. Cerium has been investigated as a possible inhibitor used as conversion coating,[49-51] applied by anodization,[52] cathodic polarization,[46,47] or long exposure at open-circuit potential (OCP).[53] In some cases, the formation of the film is accelerated by an oxidizer.[46,54] Some of the methods also require thermal treatment (up to 110°C) to accelerate the film formation (e.g., Ref. 53 and 65-67). Cerium has been proposed as an inhibitor for a variety of materials, such as steel,[55] tinplate,[56] zinc,[43,44] Cu,[46-48] Al,[57] and several aluminum alloys.[49-51,58-61] At potentials where ORR takes place on Cu, it has been suggested that the initial film contains Ce(III), but as the Cu is exposed for longer

* Electrochemical Society Student Member.
** Electrochemical Society Active Member.

[a]In a recent publication,[9] ORR on Cu (in 0.1 M Na_2SO_4 solution adjusted to various pH) has been characterized. A four-electron path was reported and the measured limiting current densities were found to be independent of pH. ORR on Cu in borate solutions[10,11] have been investigated. It was suggested that Cu(I) or CuO_2 might be present and suppress ORR even at negative potential values where mass transfer control should be significant, hence a mix control could be observed in a larger portion of E-log*i* curve. However, an almost ideal limiting current density predicted by the Levich equation was observed at the most negative potential and could be extracted from the Koutecky-Levich (KL) approach.[11] Additionally, an earlier publication[12] described the oxygen kinetics on AA2024-T3. The current was found to be smaller than ideal Levich behavior, but still somewhat dependent on rotation rate[13-16] (in the solution tested).

times, Ce(III) ions are oxidized to Ce(IV).[46] However, a detailed investigation of ORR kinetics which separate the effects of Ce on charge transfer and mass transfer is still needed.

Very little work has been reported on Co as an inhibitor.[42,62,63] $CoCl_2$ treatment on AA7075 after 20 days decreased the corrosion rate by about six times compared to an untreated alloy.[42] It was found that the product formed was a mixed Al/Co oxide. Patents[63] were recently issued on cobalt-based conversion coatings. A cobalt(III) hexacoordinated complex {e.g., $[Co(NH_3)_6](SO_4)_3$} reacted with the aluminum surface. Several cobalt oxides (CoO, Co_3O_4, and Co_2O_3) were reported to be present. The formation of these cobalt-based coatings required heat treatment (at ~60°C) for short periods of time (5-30 min). H_2O_2 is required to form Co^{3+}.[63] $CoSO_4$ treatment at room temperature[62] produces a very modest reduction in corrosion rate, perhaps due to the very short time of exposure in $CoSO_4$ solution. The above results suggest that Co^{2+} could act as an inhibitor. However, further research is needed to understand possible inhibiting mechanisms.

The required critical concentrations of Ce, Mo, and Co to inhibit corrosion of 2024-T3 at various amounts of chloride present on AA2024[14] were recently discussed, but the fundamental electrochemical behavior of Co, Ce, and Mo on Cu was not addressed. This study seeks to determine if these ions can inhibit oxygen reduction on Cu and to grade their performance. ORR kinetics were investigated on high-purity Cu and Au in the standard RDE configuration. Gold was chosen as an ideal electrode which does not form an oxide film nor undergo corrosion. Cu was selected to mimic replated Cu or Cu-rich particles on AA2024. Potentiodynamic polarization using RDE at several rotation rates was conducted to develop cathodic E-log i data. Three inhibitor solutions were investigated: 0.1 M Na_2MoO_4, 0.1 M $CoSO_4$, and 0.05 M $Ce(CH_3COO)_3$.

Experimental

Introduction.— Rotating disk electrode (RDE) experiments were used to characterize ORR kinetics. The performance of three inhibitors toward hindering ORR kinetics in the charge transfer, mixed, and mass transport controlled regimes was determined. The experiments were performed using a standard three-electrode electrochemical cell. Pt mesh was used as the counterelectrode, and $Hg/Hg_2SO_4/K_2SO_4$(sat.) was used as the reference electrode. All potential values were converted and reported against a saturated calomel electrode (SCE). Electrochemical control was provided by an EG&G Par 273 potentiostat connected to a personal computer. A model ASR2 Pine Instrument analytical rotator was used to control the angular velocities.

Materials.— The working electrode was either Cu or Au. Cu was used to simulate Cu-rich sites on Al-Cu alloys, and Au to avoid extensive anodic current densities and interference by oxide films. Rotating disk electrodes were machined out of 99.999% Cu rods (5 mm diameter with a nominal area of 0.196 cm^2) or 99.9985% Au rods (3 mm diameter with a nominal area of 0.071 cm^2). These materials were cast into a plexiglass casing. Samples were wet-ground to a 1200-grit surface finish with silicon carbide (SiC) paper and rinsed with nanopure water (18.2 MΩ) before each test began. An area factor of 1.3 was empirically obtained and subsequently used to correct for surface roughness. The measured currents were, therefore, divided by 1.3 times the nominal area to obtain the true current densities.

The cathodic polarizations were performed in non-deaerated borate buffer solutions of alkaline pH (in the range of pH 7-11, prepared using 0.05 M boric acid adjusted to the desired pH with NaOH). These solutions were used to minimize the pH variations at the surface of the working electrode during polarization.

Inhibitor pretreatments.— The pretreatments were carried out in the following solutions: 0.1 M Na_2MoO_4, 0.1 M $CoSO_4$, and 0.05 M $Ce(CH_3COO)_3$ at room temperature. These concentrations are greater than the critical concentrations for suppression of Cu replating on AA2024-T3.[14] Cu RDE samples were pretreated in one of these solutions for a certain period of time (usually 4 h, and in some cases 12 h). During the pretreament, the potential was held at $-0.5\ V_{SCE}$ or $-0.7\ V_{SCE}$ to mimic galvanic coupling of Cu-rich phases to an Al-rich matrix when such phases are embedded in Al-Cu-Mg alloys. These treatment potentials were selected because they are within the open circuit potential (OCP) range of AA2024-T3 in near-neutral NaCl solution.[6] No rotation took place during the pretreatments.

Cathodic polarizations after inhibitor pretreatments.— Following the pretreatment period, the electrode was removed from the cell and was immersed (within 5 min) in another cell containing a borate buffer solution (of pH 7, 8.2, or 9.5). Only the borate solution used following the Mo treatment contained the inhibitor (0.1 M Na_2MoO_4); additional tests were conducted in buffer solutions of pH 7.5 and 11. A current stabilization period of 10 min preceded the cathodic polarization, which was performed from the pretreatment potential ($-0.5\ V_{SCE}$ or $-0.7\ V_{SCE}$) to $-1.2\ V_{SCE}$ at a sweep rate of 0.1 mV/s. Rotation started during the stabilization period. Usually less than 15 min elapsed between the conclusion of the pretreatment and the start of the polarization scan in the second cell.

The tests that followed the pretreatments can be grouped into two sets. One consisted of tests in which a constant rotation speed of 1000 rpm was used to investigate the effect of varying solution pH on the kinetics of ORR on Cu. The second set involved tests at several rotation rates on separate specimens (usually 100, 1000, and 3000 rpm) and was performed at a selected pH value. Additionally, control tests were conducted for a selected number of cases, in which the pretreatment solution was replaced by inhibitor-free borate buffer solution. The Cu RDE was then held at a certain potential ($-0.5\ V_{SCE}$ or $-0.7\ V_{SCE}$) for the same amount of time as the corresponding pretreatment. The Cu control test was repeated both after air transfer and with constant immersion.

ORR kinetics experiments to determine typical i_{dl}.— Additionally, a set of experiments was conducted to determine the i_{act}, i_{dl}, and k value (where $i_{dl} = k\omega^{1/2}$) from the Levich equation[74] for both Cu and Au in a similar manner as the control tests described above. These tests were run at rotation rates from 0 to 3000 rpm. The electrode was held for only 1.5 h at $-0.45\ V_{SCE}$ in pH 8.2 borate buffer solution. The rotation of the electrode started at the same time as the potentiostatic hold, followed by a cathodic potentiodynamic polarization scan.

Results

The oxygen reduction reaction on Au and Cu in the absence of inhibitors.—Figure 1 shows cathodic polarization curves (*E-i*) for tests conducted on Cu (Fig. 1a) or Au (Fig. 1b) in naturally aerated (pH 8.2) borate buffer solution at various rotation rates. The ORR reaction appears to be under mixed control on Cu. A well-defined diffusion current density (i_{dl}) is observed at $\sim -1.0\ V_{SCE}$ on tests run at speeds lower than 1000 rpm. In the case of Cu, the cathodic reaction appears to be ORR through a four-electron process, and at more negative potentials ($\sim -1.2\ V_{SCE}$) the hydrogen evolution reaction (HER) is significant. By comparison, the ORR on Au follows a two-electron reaction path at intermediate potentials with a transition to a four-electron path at potentials more negative than $-0.7\ V_{SCE}$. Moreover, the HER is significant on Au at potentials more positive than on Cu ($\sim -1.05\ V_{SCE}$). In the case of Au, the ORR is also potential-dependent over a potential range where constant i_{dl} is usually observed assuming a fixed reaction mechanism. This *E-i* shape might be due to the transition from a two-electron path to a four-electron one. The two- to four-electron path is well-established in the literature[75] for the ORR process on Au.[11,46] Hence, for both cases, there is a need to isolate i_{dl} from i_{ct}, the charge-transfer current density.

To obtain the i_{dl} value, the Koutecky-Levich[74,76] approach was used. Contributions to the total current (i_{total}) from charge-transfer

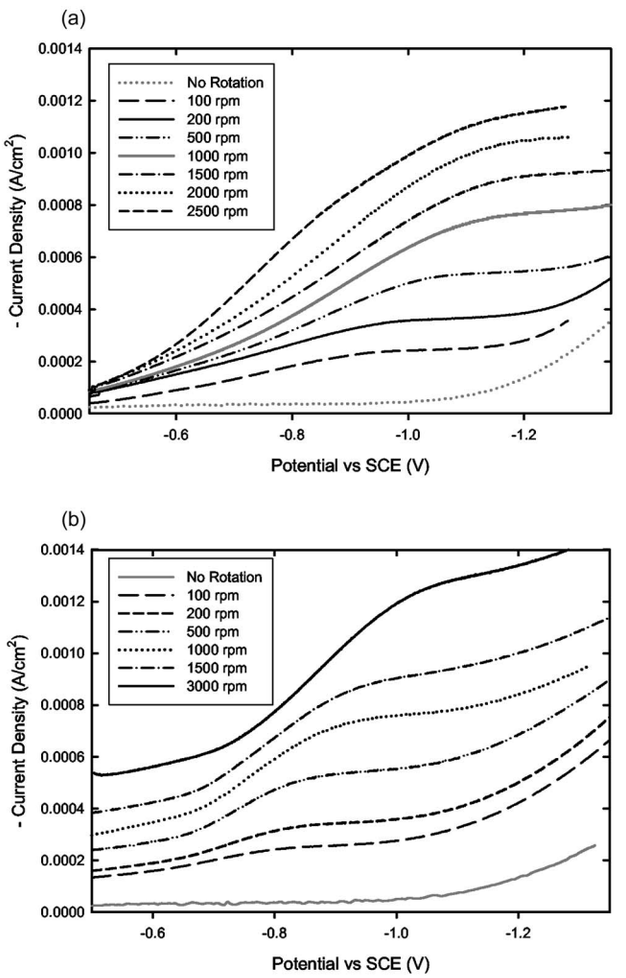

Figure 1. Oxygen reduction reaction rate during cathodic polarization (scan rate 0.1 mV s^{-1}). (1.a) On Cu at rotation rates (rpm) of (a) 100; (b) 200; (c) 500; (d) 1000; (e) 1500; (f) 2000; (g) 2500. (1.b) On Au at rotation rates (rpm) of (a) 100; (b) 200; (c) 500; (d) 1000; (e) 1500; (f) 3000.

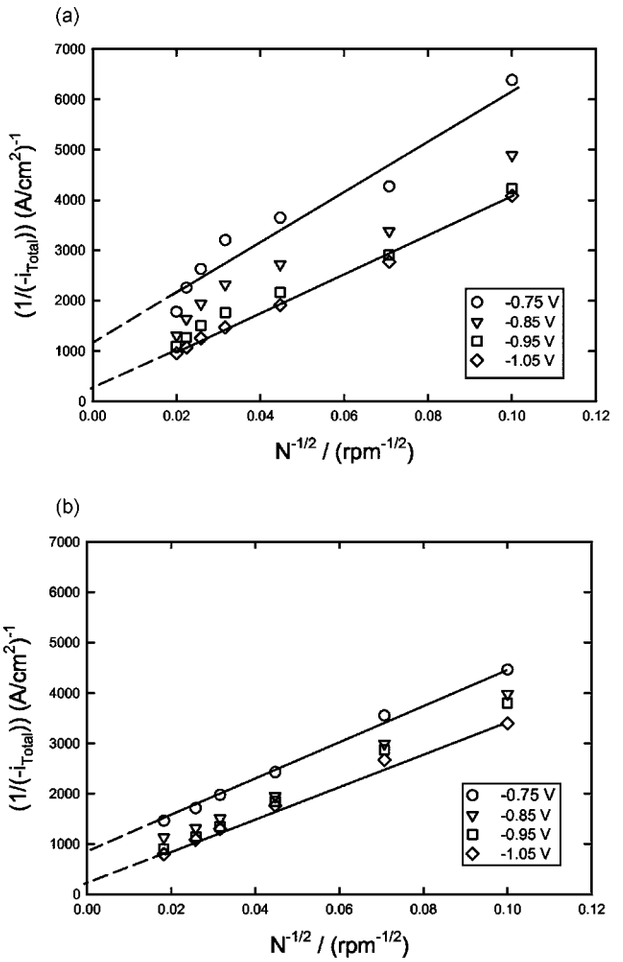

Figure 2. Koutecky-Levich plots (a) Cu, (b) Au. Oxygen reduction currents are reported at potentials from top to bottom −0.75 to −1.05 V. Analysis of $E - i_{total}$ results obtained on RDE, in the region of mixed control. The activation controlled current density is obtained from the intercept of the lines at infinite rotation rate ($N^{-1/2} = 0$).

current (i_{ct}) were obtained from Koutecky-Levich plots shown in Fig. 2a and b. The intersection of the trendline of $1/(-i_{total})$ vs $N^{-1/2}$ (where N is disk rotation rate in rpm) with the y axis gives a good estimate of $1/i_{ct}$ for each of the lines shown. Equation 1 was used to obtain the corresponding diffusion limited current density (i_{dl}) for each case, where $i_{dl} = kN^{1/2}$, where $N \propto \omega/2\pi$/cycle

$$\frac{1}{i_{total}} = \frac{1}{i_{ct}} + \frac{1}{i_{dl}} \quad [1]$$

Figure 3 shows i_{total} values (right y axis) and the extracted i_{dl} values (left y axis) as a function of the square root of the disk rotation rate ($\omega^{1/2}$) (abscissa) for selected potential values on Cu (Fig. 3a) as well as on Au in the four-electron regime (Fig. 3b). These extracted i_{dl} values were obtained using Eq. 1. Figure 3 also includes the theoretical Levich prediction of i_{dl} for 7 and 8 ppm (continuous lines). The Levich equation[74] (Eq. 2) was used to calculate these theoretical values for the mass transport limited ORR

$$i_{dl} = 0.62\, nFD^{2/3}\nu^{1/6}C\omega^{1/2} \quad [2]$$

In Eq. 2, n is the number of electrons transferred to complete the half cell reaction taken as 4; F is Faraday's constant; D is the diffusion coefficient for dissolved O_2 assumed to be 1.9×10^{-5} cm^2/s;[77] ν is the kinetic viscosity assumed to be 0.01 cm^2/s;[78] ω is the disk rotation rate (rad/s); and C is the concentration of oxygen in the bulk solution. $C = 2.193 \times 10^{-7}$ mol cm^{-3} (7 ppm) and $C = 2.5 \times 10^{-7}$ mol cm^{-3} (8 ppm) were the assumed values for the computations. The slope (K_o) of these theoretical lines where $i_{dl} = K_o\omega^{1/2}$ is 81.23×10^{-6}A $s^{1/2}/rad^{1/2}$ cm^2 and 92.83×10^{-6}A $s^{1/2}/rad^{1/2}$ cm^2 for 7 and 8 ppm O_2, respectively. Table I summarizes the slopes (K_o) fitted for the data shown in Fig. 3 corresponding to both materials. The averages $K_o = 83.1$ A $s^{1/2}/rad^{1/2}$ cm^2 (not including K_o for -0.75 V_{SCE}) for Cu and $K_o = 85.1$ A $s^{1/2}/rad^{1/2}$ cm^2 (not including K_o for -1.05 V_{SCE}) for Au are in agreement with reported values.[9] These K_o values suggest that the O_2 concentration in the solution was 7 ppm and match the theoretical values from Eq. 2 for a four-electron reduction process. These results indicate that a four-electron ORR mechanism takes place on Cu and on Au in natural aerated borate solution at potential values ranging from -0.75 V_{SCE} to -1.05 V_{SCE}. In general, i_{dl} values on Au are slightly larger than on Cu for corresponding sets of conditions, possibly due to the presence of Cu oxides. These results were used for comparison to the data obtained after inhibitor treatment.

Oxygen reduction reaction kinetics after inhibitors pretreatments.—As indicated in the Experimental section, three different pretreatments were investigated. Rather than name the salt

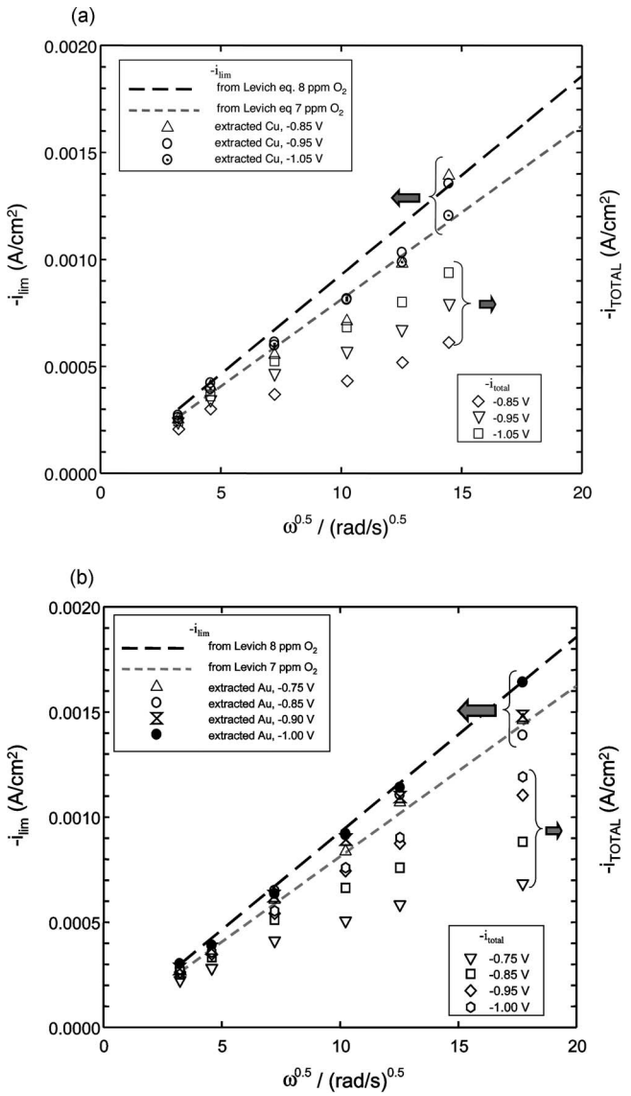

Figure 3. Rotation rate dependence of the mass-transport limited current density on Cu (a) and on Au (b). The dotted lines indicate ideal Levich behavior for 7 and 8 ppm dissolved O_2 concentration.

and its concentration in the solutions, throughout the text, the active component is indicated (in other words, Ce, Co, or Mo) by referring to Ce(III), Co(II), or Mo(VI).

Table I. K_o and R^2 values for Cu and Au at various potentials from cathodic polarization scans. For mass transport limited ORR in borate buffer solution at pH 8.2. $i_{dl} = K_o\omega^{1/2}$ was fitted after extraction of i_{dl} from K-L plot.

	Cu		Au	
Potential (V)	K_o (A $s^{1/2}$/rad$^{1/2}$ cm^2)	R^2	K_o (A $s^{1/2}$/rad$^{1/2}$$cm^2$)	R^2
−0.750	67.81	0.908	83.04	0.998
−0.800	78.23	0.906	84.18	0.987
−0.850	83.51	0.928	83.67	0.981
−0.900	85.82	0.955	83.31	0.988
−0.950	86.57	0.975	85.37	0.997
−1.000	83.11	0.99	91.12	0.998
−1.050	81.23	0.996	102.1	0.986

Effect of pretreatment exposure time tested at a constant rotation rate.—Figure 4 shows sets of cathodic polarization *E-i* curves obtained on Cu in pH 8.2 (Fig. 4a-c) and pH 9.5 (Fig. 4d) borate buffer solutions after pretreating the sample for 4 or 12 h in one of the three inhibiting solutions. Figure 4a shows cathodic *E-i* curves obtained in pH 8.2 borate solutions after 4 h of pretreatment in inhibitor solutions. A curve corresponding to an untreated control test described above is also included. Additionally, a curve corresponding to a similar control test is also shown in which the sample was removed after the potential hold for a brief period of time (<5 min) from the solution and then immersed again to conduct the polarization. This shows that removing the sample of the solution while conducting the control test does not affect the cathodic kinetics. In each inhibitor treated case, a decrease in the cathodic ORR kinetics is observed to different degrees. The cathodic kinetics on Cu after Co and Ce treatments are consistent with film precipitation on a homogeneous electrode as discussed below. In contrast, the abatement in the cathodic kinetics after Mo treatment takes on an unusual shape. The ORR current decreased abruptly at a potential of -0.8 V_{SCE} (a change in the current direction might have started with the inflection taking place at -0.75 V_{SCE}). However, a valley is observed and the current started to increase at ~ -0.85 V_{SCE}. The potential where the reaction rate decrease occurs is in agreement with the Mo(VI) → Mo(IV) reduction reaction (more details will follow in the Discussion section). This complex shape might be due to chemisorption of Mo(VI) followed by its electrochemical reduction to form a covering (oxide) film. The subsequent rise in cathodic reaction rate could be a result of enhanced solubility of this film due to pH rise or film reduction.

It can be seen that the Ce pretreatment stifles the cathodic ORR kinetics on Cu. Previous authors[46,48] have shown that the precipitate is a surface film that acts as a cathodic inhibitor layer. Oxygen reduction is stifled more rapidly and more effectively on Cu held at -0.56 V_{SCE} compared to -0.85 V_{SCE} when testing in a solution that contains Ce while holding the potential and rotating at 1000 rpm.[46] In this study, the curve corresponding to the sample subject to Ce treatment and potentiostatically held at -0.7 V_{SCE} (Fig. 4b) performed the best compared to the other Ce pretreatment at -0.5 V_{SCE} (Fig. 4a). Both Mo and the Ce pretreatment at -0.5 V_{SCE} are second best in performance (Fig. 4a). Between these tests, no major difference in the measured ORR current is observed for the range -0.95 V_{SCE} to -1.05 V_{SCE}, but from -0.8 V_{SCE} to -0.95 V_{SCE} the Mo treatment performed better than the Ce treatment at -0.5 V_{SCE}. The least cathodic inhibition was found in the case of Co treatment. Oxygen reduction *E-*i_{total} behavior after Co treatment was below the control curves but not by a large amount.

Figure 4c shows test results after 12 h pretreatment. As in Fig. 4a, Fig. 4c includes an untreated control test, but it also includes a modified control test produced by holding the sample at -0.45 V_{SCE} for only 1 h. Similar inhibitor performance is observed in Fig. 4c as in Fig. 4a. In Fig. 4c, the curve following the Ce pretreatment displays the smallest current density. The curve following Mo pretreatment has larger current density than the control until about -0.75 V_{SCE}, where the current density drops abruptly with further cathodic potential. For potentials lower than -0.825 V_{SCE}, the measured current after Mo treatment is smaller than the one measured on untreated Cu (12 h potential hold).

In the case of Co after 12 h hold, the corresponding *E-*i_{total} curve is above the *E-*i_{total} curve corresponding to the control case after analogous 12 h hold, but below the 1 h control curve at a rotation rate of 1000 rpm. The 12-h-long potential hold allows the formation of a Cu oxide on the Cu surface[11] that apparently lowers its cathodic kinetics more than the Co treatment does. It is speculated that such inhibitor pretreatments, while forming a homogeneously Co precipitated film, might prevent the Cu oxide formation.

The measured current density on a stationary Cu electrode at the end of the pretreatment period in the Co inhibiting solution is significantly smaller on Cu (not shown) than the current measured at the beginning of the polarization after transferring the Cu RDE to

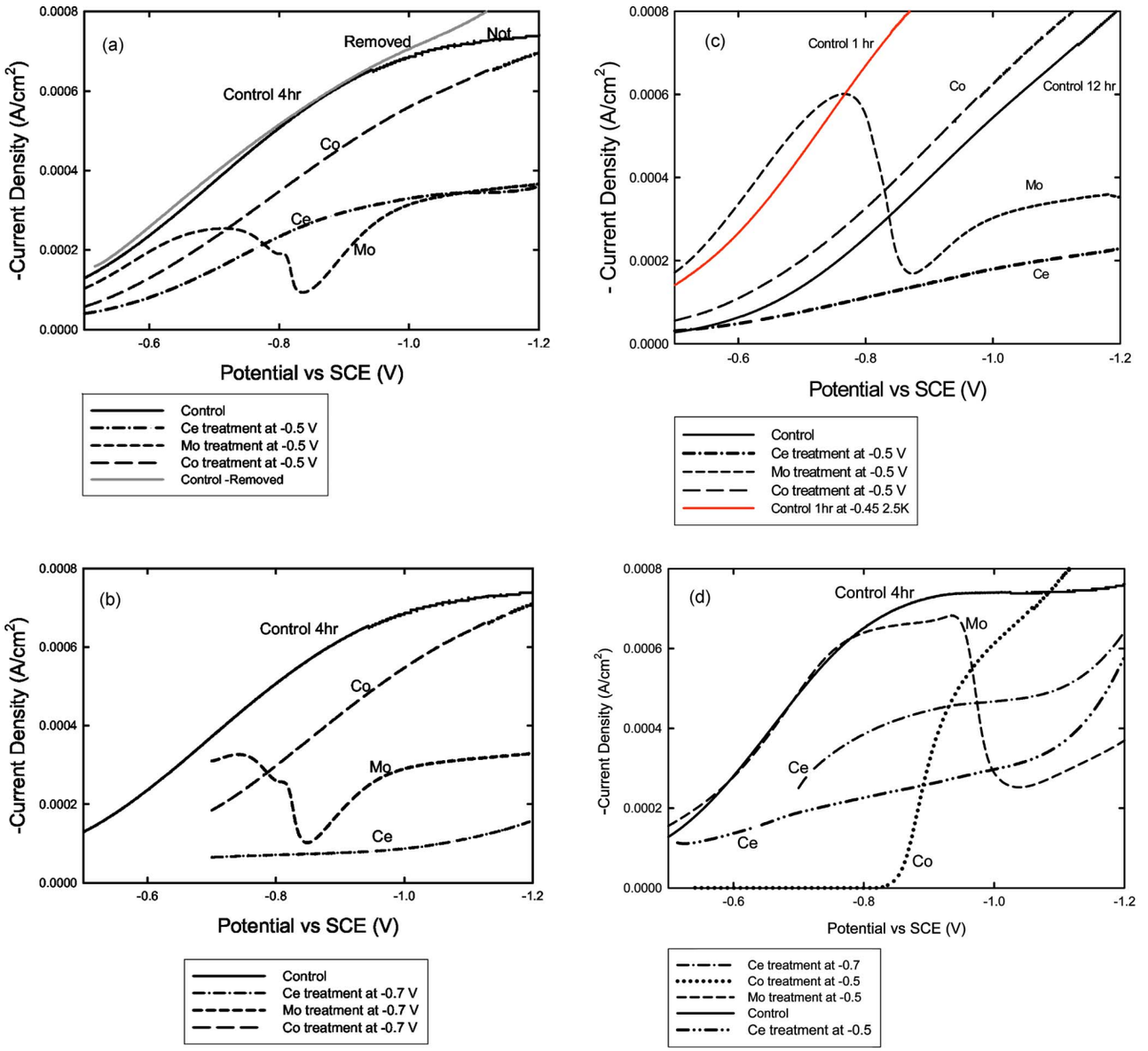

Figure 4. ORR current density vs applied potential for Cu RDE electrodes. (a) Samples potentiostatically held for 4 h at −0.5 V in the inhibitor solution (no rotation), transfered to pH 8.2 borate buffer solution, held for 10 min at the same hold potential followed by a potential sweep at 1000 rpm. (b) As (a) but samples potentiostatically held for 4 h at −0.7 V. (c) Samples potentiostatically held for 12 h at −0.5 V in the inhibitor solution, potential sweep at 3000; (d) as (a) but transfered to pH 9.5 borate buffer solution with potential sweep at 1000 rpm. Test that followed Mo treatment also contained 0.1 M Na_2MoO_4 in the solution.

the borate solution and beginning rotation. The measured current density is also reduced during Ce pretreatment of a stationary electrode. It is possible that when the sample is transferred to pH 8.2 borate solution, the conditions are not thermodynamically as favorable for $Co(OH)_2$ precipitation as during pretreatment in the unbuffered solution. The pH rise is speculated to be greater in the unbuffered pretreatment solution during ORR compared to the buffered solution used to evaluate the ORR kinetics. Thus the Co film formed during treatment is lost by chemical dissolution in the slightly less alkaline pH 8.2 solution.[73]

Tests in pH 9.5 borate solution were conducted in order to confirm the possible pH dependent behavior observed on *E-i* curves. Figure 4d shows tests conducted in borate solution at pH 9.5 for the control and after each of the three pretreatments. For this set of tests, Co pretreatment reduced the current density the most, until $\sim -0.86\ V_{SCE}$, where the current started to increase exponentially. In contrast, the current densities measured on Cu after Ce and Mo treatments were larger when tested in (pH 9.5) borate solution than in the case of (pH 8.2) borate solution. In the case of the test that followed Mo treatment, the curve shows that both the potential at which the speculated Mo(VI) chemisorption starts (decrease in current density) and its abrupt reduction (valley) are shifted toward more negative potential values with increasing pH. The *E-i* curves following Ce treatment are not very different from those shown in Fig. 4a-c at pH of 8.2.

Effect of rotation rate on the oxygen reduction reaction kinetics.—Figure 5a-c shows cathodic polarization curves after pretreatments in Ce, Mo, and Co containing unbuffered solutions, respectively, at various rotation rates. For comparison, all the above

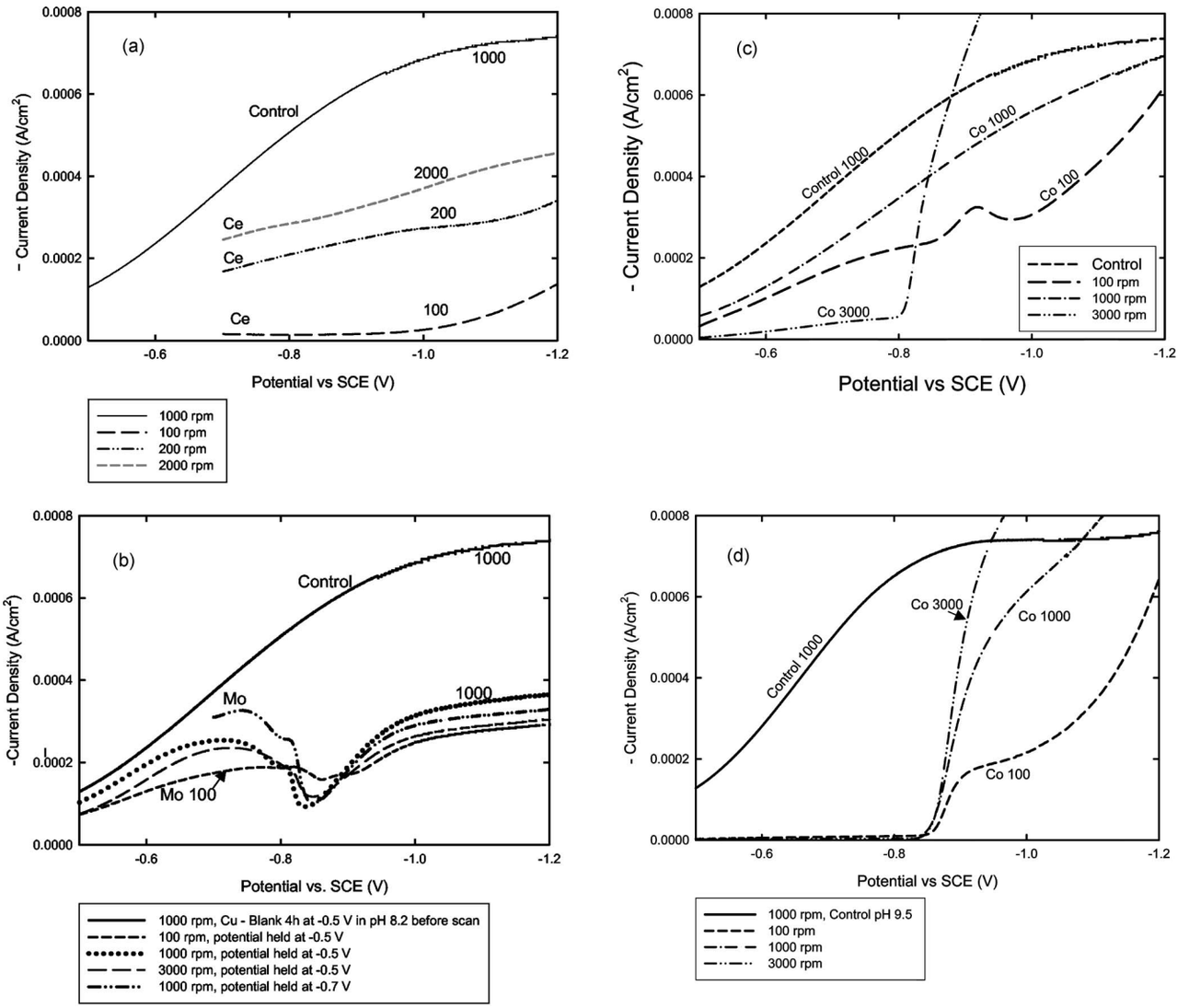

Figure 5. ORR current density vs applied potential for Cu RDE electrodes. Samples potentiostatically held for 4 h at either −0.5 or −0.7 V in the inhibitor solution (no rotation), transferred to pH 8.2 or pH 9.5 borate buffer solution, held for 10 min at the same hold potential followed by a potential sweep at the indicated rotation rates (rpm). (a) followed Ce pretreatment, pH 8.2; (b) Mo pretreatment, pH 8.2 solution also contained 0.1 M Na_2MoO_4; (c) Co pretreatment, pH 8.2; (d) Co pretreatment, pH 9.5.

figures also included the control scan run at 1000 rpm in the pH 8.2 borate buffer. In Fig. 5a, the current density over the potential range of interest is significantly smaller for the test conducted at 100 rpm. The fact that the current density values corresponding to the curves at 200 and 2000 rpm are close to each other suggests that the i_{dl} values do not follow theoretical Levich behavior. That is to say, ORR is not controlled by hydrodynamic properties of the solution. Figure 5b shows that there is no significant difference between *E-i* behavior at different rotation rates in a series of tests after the Mo pretreatment. The change in *E-i* slope (at ~ -0.75 V_{SCE}) and the valley (at ~ -0.82 V_{SCE}) is observed at approximately the same potential values in all cases. Figure 5c shows curves after pretreatment in Co. Here, the current density measured for the test run at 100 rpm is somewhat smaller than that for the test run at 1000 or 3000 rpm. Figure 5d shows the effect of rotation rate on Co treated electrodes as in Fig. 5c, but for cases run in pH 9.5 solution rather than pH 8.2 solution. For the curves shown in Fig. 5d, the current density is again negligible until the polarization reaches ~ -0.85 V_{SCE}, at which point the current increases exponentially, with the largest current corresponding to the test conducted at the fastest rotation.

As the 100 rpm cathodic polarization curve indicates in Fig. 5a, Ce pretreatment can reduce the cathodic kinetics significantly. However, when rotation speed is increased, the abatement of the cathodic kinetics is not as large. To investigate whether there is a transient limitation in the amount of precipitate that can remain present at the electrode surface due to high flow-induced shear stress, a potentiostatic experiment was conducted after performing cathodic polarization at 100 rpm in pH 8.2. The Cu electrode was held at -0.95 V_{SCE}, the rotation was stopped, and the current monitored until a stable reading was obtained. The rotation rate was progressively increased after a hold period. Figure 6 shows the result of this test on the ORR rate at -0.95 V_{SCE}, along with the corresponding rotation rates (on the right *y* axis). Interestingly, the current increased very little with incremental increase in the rotation rate when the film was first allowed to form at low rotation rate (100 rpm).

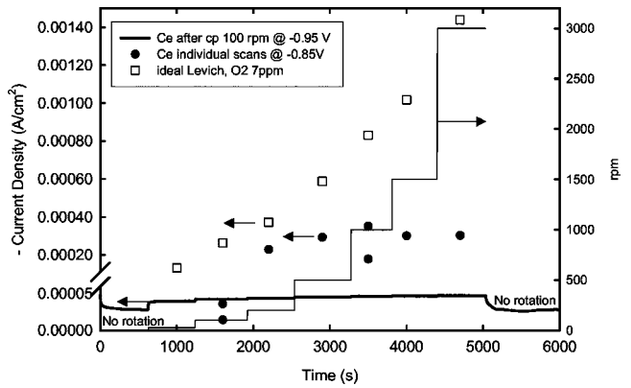

Figure 6. Chronoamperometic curve (current vs time) for Cu RDE at a constant potential of −0.95 V. Several rotation rates were investigated. The test was conducted after Ce pretreatment. Current densities from individual scans and ideal Levich current density values are also included.

Effect of pH on the oxygen reduction reaction kinetics.— Given the complex ORR kinetics observed, experiments were repeated at various pH levels as a diagnostic procedure to gain more insight. Sets of cathodic polarization tests were conducted at various pH levels at selected rotation rates after 4 h pretreatment in the inhibitor solutions. Figure 7a shows curves obtained at 1000 rpm after pretreatment in Ce. The E-i_{total} curve with the smallest current densities corresponds to the test conducted in pH 7, followed by the E-i_{total} curve test conducted in pH 8.2 solutions. The profiles of tests conducted in (pH 8.2) borate solution show considerable variability between cathodic polarization scans. The test run in pH 9.5 borate solution has the largest current density of the four tests conducted. All the polarization curves corresponding to the Ce pretreatments were below the control as shown. When similar tests were conducted at 100 rpm, the observed current densities were small for the tests run in solutions of pH 8.7 or lower, whereas current densities for tests conducted in pH 9.6 were once again slightly larger. In summary, the cathodic kinetics are reduced for Ce, but all Ce treatments were better at less alkaline pH values. This could be speculatively associated with the morphology of the $Ce(OH)_3$ or CeO_2 deposit.

For the scans run after Mo treatment at different pH levels, it is important to note that if the pH is below 8, the solubility of MoO_2 is low.[73] Figure 7b shows reduction in cathodic kinetics at pH 7.0 and 7.6. However, no abrupt drop in current density is seen. One interpretation is that hydrogen evolution reaction (HER) masks any benefit of Mo on ORR at these more acidic pH values. At pH 8.2 and 9.5 an abrupt drop is seen in cathodic current density near −0.8 V_{SCE} and −1.0 V_{SCE}, respectively. A valley is still observed at pH 9.5. However, above −0.8 V_{SCE}, the current density values are almost identical to the control values. For the test conducted at pH 11, no valley is observed in the potential range of interest shown in the figure. It will be shown below that this abrupt pH dependent decrease in current density (i.e., valley) can be explained by Mo(VI) reduction to Mo(IV) given the pH dependence of this reaction

$$MoO_4^{2-} + 4H^+ + 2e^- \rightarrow MoO_2 + 2H_2O \quad [3]$$

$$E_{[Mo(VI)/MoO_2],NHE} = 0.606 - 0.1182\ pH + 0.0295\ \log[MoO_4^{2-}] \quad [4]$$

The position of the valleys corresponding to tests conducted in solutions of pH ranging from 7 to 11 were plotted against the Nernst potentials for the MoO_2 formation reaction given in Eq. 4 and the Nernst potential of HER (H_2/H^+) assuming a Na_2MoO_4 concentration of 0.1 M. Figure 8 shows the relationship between the experimentally observed potential for the E-i valleys and Nernst potentials

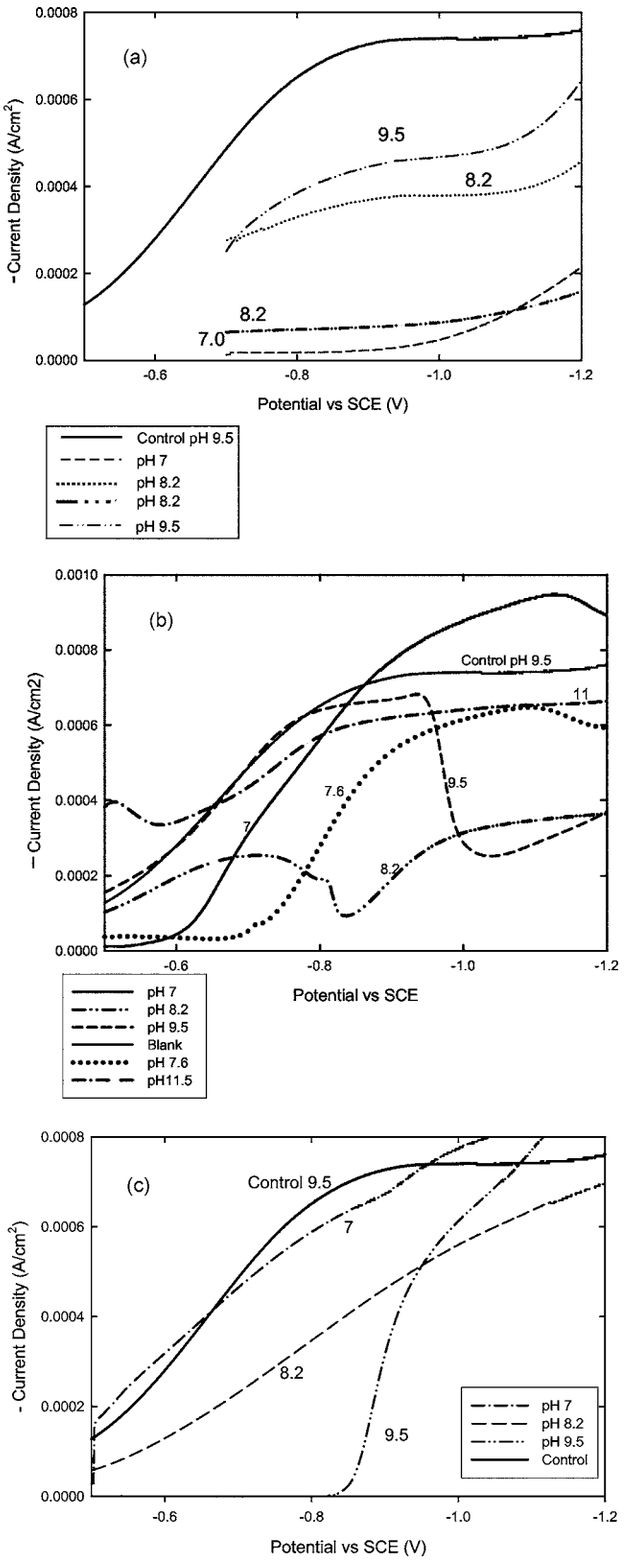

Figure 7. ORR current density vs applied potential for Cu RDE. Samples potentiostatically held for 4 h at either −0.5 or −0.7 V in the inhibitor solution (no rotation), transferred to borate buffer solution of pH as indicated by each curve, held for 10 min at the same potential as treatment and followed by a potential sweep at 1000 rpm. (a) Ce pretreatment; (b) Mo pretreatment, solutions also contained 0.1 M Na_2MoO_4; (c) Co pretreatment.

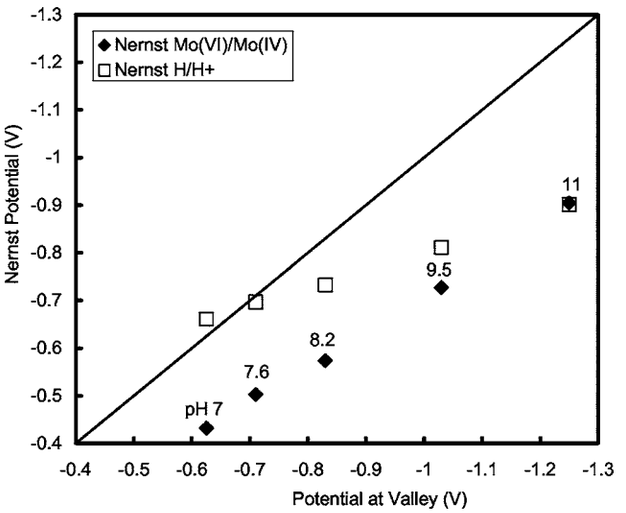

Figure 8. Valley potential from cathodic scan following Mo treatments vs Nernst potentials for Mo(VI)/(IV) and (H_2/H^+) reduction reactions (SCE scale) and 1:1 line.

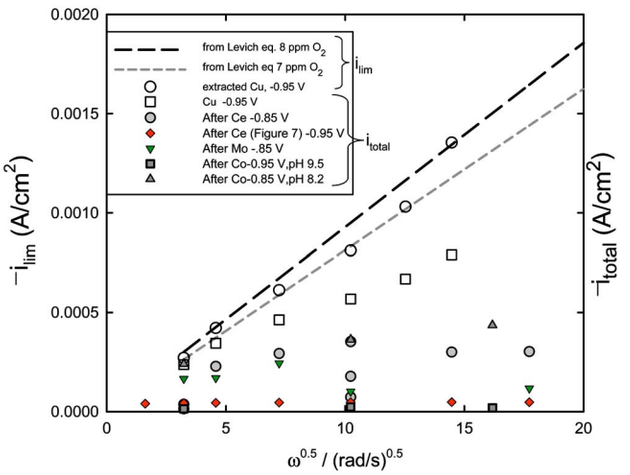

Figure 10. Rotation rate dependence of the mass-transport limited current density on bare Cu (control) and Cu pretreated in different inhibitor solutions: Ce(III) from individual scans, Ce(III) from chronoamperometric at −0.95 V, Mo(IV), Co(II) tested in pH 8.2 borate solution, and Co(II) tested in pH 9.5 borate solution.

for Mo(VI) reduction to MoO_2. Both series appear to have a linear relation and a similar dependency on pH. The position of the valley potentials is below (more negative than) the corresponding Nernst potential for the Mo(VI)/Mo(IV) process indicative of thermodynamic consistency with this reaction. The Nernst potentials of H_2/H^+ were more negative than the Nernst potentials for Mo(VI)/Mo(IV) reaction except at pH $>$ 8.2, where the difference becomes very small. These findings strongly suggest that a MoO_2 film caused the valley in *E-i* behavior with some thermodynamic irreversibility. The current increases at more negative potentials as a result of both HER, and also due to the potential driven reduction or pH driven oxidation[73] of the film.

Figure 7c shows that considerable cathodic reaction suppression is observed after Co pretreatment as the pH increases. The results are significant, since suppression of cathodic kinetics by Co is small at other pH levels. These results will also be interpreted in the discussion.

Oxygen reduction reaction kinetics comparison: With inhibitor pretreatments vs no pretreatment.—Figure 9 repeats a selected portion of the data shown in Fig. 2a, but Fig. 9 also includes $1/(-i_{total})$ values for results obtained at −0.85 V_{SCE} from the polarization curves conducted after pretreatment. Moreover, Fig. 9 also shows a data series obtained from the curve shown in Fig. 6. All the results after inhibitor pretreatments yield current densities that are relatively independent of rotation rate with the exception of the Co pretreatment followed by testing in pH 8.2 borate solution. Since inhibitor pretreatment results in a deviation from simple mixed control, it is likely that Eq. 1 cannot be used to extract i_{dl} values because it is an incorrect model. It also suggests that i_{act} in case of pretreatments is lower than i_{act} on bare Cu and that i_{total} becomes rotation-rate-independent.

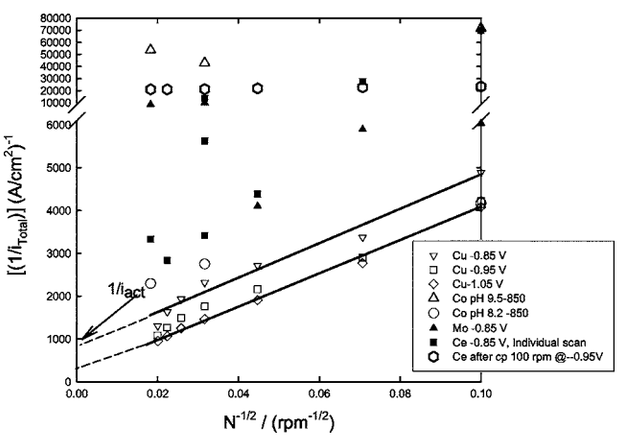

Figure 9. Koutecky-Levich plots of tests conducted on Cu after pretreatment in different inhibitor solutions.

Figure 10 shows extracted values of i_{dl} (left) and i_{total} (right) for bare Cu shown in Fig. 3a. Additionally, Fig. 10 shows i_{total} after the pretreatments. The results indicate that the best ORR inhibition is achieved after Co pretreatment in pH 9.5 borate solution. The next best is the Ce pretreatment (after 100 rpm test, ♦ tested at 8.2 pH). The current densities measured (i_{total}) in pH 8.2 borate solution after Co treatment are only slightly smaller than currents measured at −0.85 V_{SCE} in the control tests (which were subject to potential hold for 1 h). In summary, Co reduces the cathodic kinetics the most when tested in a more alkaline solution (pH 9.5) compared to pH 8.2 and 7. Ce pretreatment gives the best result in less alkaline solutions (pH 8.2 and 7) after Ce pretreatment at −0.7 V_{SCE} (Fig. 6). In contrast, Mo was most effective when tested in pH 8.2 borate solution and became ineffective at pH 11.

Discussion

Oxygen reduction reaction.— In non-deaerated solutions, the cathodic reaction in a corroding Al precipitation age hardened alloy system is the reduction of the dissolved oxygen. This reaction can occur via two pathways depending on the nature of the metal substrate and the presence or absence of an oxide film.[46] One mechanism is an overall four-electron process. This reaction takes place in two steps.[73] The first step is the formation of hydrogen peroxide, which, under alkaline conditions, can be written as[46]

$$O_2 + 2H_2O + 2e^- \rightarrow H_2O_2 + 2\ OH^- \quad [5]$$

The second step is the formation of hydroxide ions

$$H_2O_2 + 2e^- \rightarrow 2\ OH^- \quad [6]$$

The overall reaction is

$$O_2 + 2H_2O + 4e^- \rightarrow 4\,OH^- \quad [7]$$

The equations above suggest the possibility of at least the transient formation of peroxide intermediates during the oxygen reduction reaction (ORR). The other pathway is a two-electron process, which leads to the direct formation of hydrogen peroxide as a product of ORR[46]

$$O_2 + 2H_2O + 2e^- \rightarrow H_2O_2 + 2\,OH^- \quad [8]$$

In the case of gold, it has been shown that the ORR mechanism is potential-dependent.[79] In alkaline solutions, the two-electron pathway is dominant at around -0.7 V_{SCE}, and the four-electron process occurs at potentials below -1.0 V_{SCE}. For copper, it was found that the overall four-electron process takes place in neutral solutions.[80] However, a small amount of hydrogen peroxide was detected when the pH of the solution reached 10.

The ORR typically becomes mass-transfer-controlled (i_{dl}) at fairly negative potentials (e.g., at and below ~ -0.7 V_{SCE}). In some cases, the electrodes were held at -0.5 V_{SCE} during pretreatments, therefore the charge-transfer regime (i_{act}) of the ORR is also important. The total cathodic current for ORR (i_{total}) under this mixed control can be described by Eq. 1. In the presence of inhibitor hydroxide, oxyhydroxide, and oxide films formed over Cu, another "resistance" term can be added to Eq. 1, which becomes

$$\frac{1}{i_{total}} = \frac{1}{i_{act}} + \frac{1}{K_o\omega^{1/2}} + \frac{1}{i_{film}} \quad [9]$$

where i_{film} is the current associated with the diffusion of oxygen through the film. This additional term leads to a low or nonexistent rotation rate dependence of the cathodic current density if $i_{film} \ll i_{act}$ and $i_{film} < K_o\omega^{1/2}$.

Model.— The formed films might act as a physical barrier that diminishes O_2 mass transport and could reduce i_{act}. The poor dependence of i_{dl} on the rotation rate (Fig. 10) might be attributed to a reduction of O_2 penetration due to film present after the treatments. The high intercept in Fig. 9 indicates a reduction of i_{act}. Equation 9 describes the total current density measured during cathodic polarization in the presence of a surface film. After exposure to the different inhibitor solutions, a film is formed on the surface of Cu. This film can be considered as an additional resistance for the diffusion of O_2. i_{dl} can be calculated by adding a term with a term that describes the transport of O_2 through the precipitate layer[15]

$$i_{dl} = \frac{nFC}{\frac{\delta_{solution}}{D_{solution}} + \frac{\delta_{film}}{D_{film}}} \quad [10]$$

where δ_{film} is the average film thickness and D_{film} the diffuson coefficient of O_2 through the film. $\delta_{solution}$ and $D_{solution}$ are the boundary layer thickness and diffusion coefficient of O_2 through the boundary layer; $\delta_{solution}$ changes with rotation rate. $D_{solution}$ is $\sim 2 \times 10^{-5}$ cm^2/s. $\delta_{film} = 1$ μm was assumed. An overall expression for the cathodic current density for O_2 reduction i_{cat} is given by Eq. 11 (neglecting HER and assuming i_{dl} defined by Eq. 10). i_{act} is also reduced as indicated by Eq. 11. An additional factor that could affect i_{dl} and i_{cat} as proposed by Kaesche[81] and Ilevbare[16] is the coverage by adsorbed ions, which reduces the effective electrode area. Competitive adsorption of anions (MoO_4^{2-}) or Ce^{3+}, Co^{2+}, Mo^{6+} species could block O_2 adsorption sites. The electrochemically active electrode area for ORR is proportional to the area that is not covered with ions. $Area_{ORR} = Area_{electrode}{}^{*}(1 - \theta_{ions})$. $Area_{ORR}$ affects both i_{dl} and i_{act}. However, to calculate θ_{ions}, the type of adsorption model that is applicable as a function of potential is needed but these parameters are unknown. Hence, such a factor was not included in Eq. 11. It was assumed that the entire electrode area was covered by a film. In this case, the ORR rate can be described as

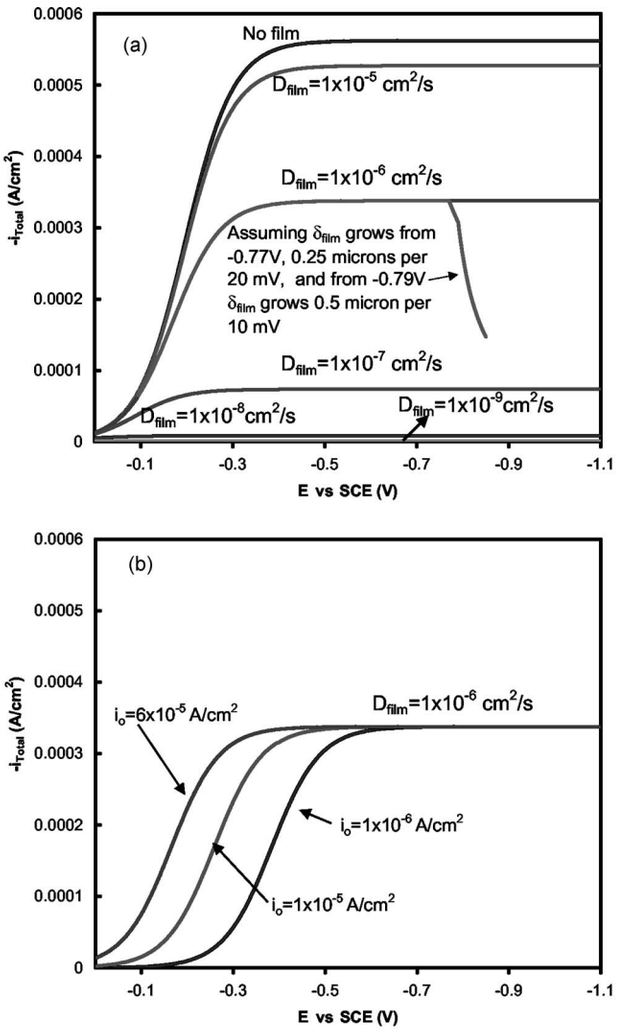

Figure 11. Theoretical ORR current density vs theoretical applied potential. (a) For different D_{film} values on a homogeneous electrode containing a precipitated film. The case with no precipitated film and the case with additional film growth due to Mo treatment are also included. (b) For a selected D_{film} and several $i_o^{O_2}$ values.

$$i_{cat} = \frac{i_o^{O_2} e^{(E_{O_2} - E)/\beta_c}}{1 + \frac{i_o^{O_2}}{i_{dl}} e^{(E_{O_2} - E)/\beta_c}} \quad [11]$$

where $i_o^{O_2}$ is the exchange current density for oxygen reduction, $(E_{O_2} - E)$ is the overpotential, and β_c is the Tafel slope for oxygen reduction. Curves generated with Eq. 11 are simplifications of the measured current. However, they can help to gain insight into the way a deposited film might modify the measured current. Theoretical polarization curves were calculated assuming $\beta_C = 120$ mV/dec, $i_o^{O_2} = 6 \times 10^{-5}$A/cm^2, $E_{O_2} = -0.04$ V_{SCE}, $D_{solution} = 2 \times 10^{-5}$ cm^2/s, D_{film} in a range between 1×10^{-5} and 1×10^{-9} cm^2/s, and a $\delta_{film} = 1$ μm, $\delta_{solution} = 28.5$ μm corresponding to $\sim$500 rpm. The curves generated are shown in Fig. 11a. The calculated curves indicate that the presence of a film suppresses the ORR below the "ideal" Levich behavior. The measured *E-i* relationships show trends similar to the ones obtained with the model (not including the valleys, which are due to an additional film formation), suggesting that the inhibitor treatments suppress ORR on Cu through a film formation. Moderate ORR suppression might indicate

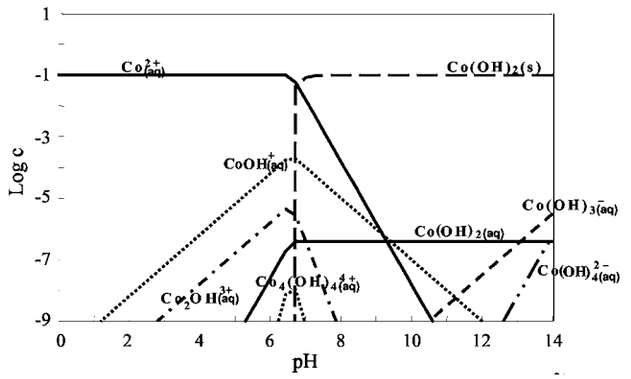

Figure 12. Logarithm of concentrations of chemical species present in a Co^{2+}-water system as a function of pH. The bulk concentration of Co^{2+} ions is 0.1 M.

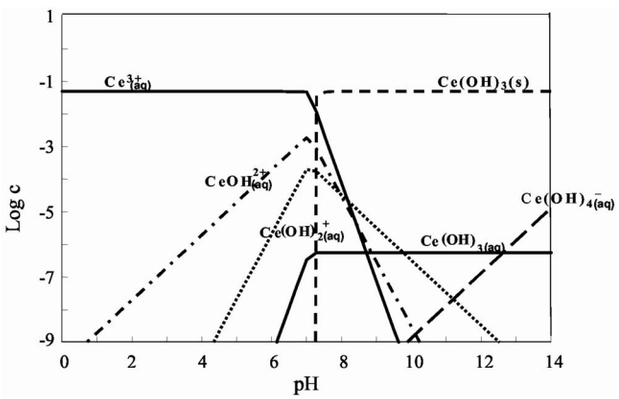

Figure 13. Logarithm of concentrations of chemical species present in a Ce^{3+}-water system. The bulk concentration of Ce^{3+} ions is 0.05 M.

D_{film} in the order of between 1×10^{-5} and 1×10^{-6} cm^2/s; $D = 1 \times 10^{-9}$ cm^2/s appears to better describe polarization curves after Co treatment conducted in pH 9.5. The case of $D_{film} = 1 \times 10^{-6}$ cm^2/s was explored further. Assuming pH 8.2, the Nernst potential of the Mo(VI)/Mo(IV) redox reaction is ~ -0.63 V_{SCE} (Eq. 4). The formation of a MoO_2 film is pH dependent and could take time and the buffer capacity might be surpassed, thus changing the pH at the electrode interface and shifting the Nernst potential. The potential at which the film growth is relevant was chosen as -0.77 V_{SCE}. The δ_{film} was assumed to grow as follows: when $E < -0.77$ V_{SCE}, δ_{film} was assumed to grow slowly (0.125 μm/10 mV) for the next 0.02 V and slightly faster for the next 0.06 V up to $\delta_{film} = 4.25$ μm. This $\delta_{film} = f(E)$ was included in Eq. 11. Figure 11 shows how the current density changes in the *E-i* curve. The MoO_2 film might dissolve upon further polarization as a result of pH and *E* changes. The simplified model seems to properly describe the *E-i* observed following the Mo treatment. Moreover, the effect of $i_o^{O_2}$ on the modeled *E-i* curve was investigated and the results are shown in Fig. 11b. The smallest $i_o^{O_2}$ delays the charge-transfer portion of the curve by ~ 200 mV when compared to the larger $i_o^{O_2}$ value, which is expected due to the ~ 1.5 orders of magnitude difference between them.

Effect of inhibitors on ORR.— In case of the Co(II) and Ce(III) pretreatments on Cu in 0.1 M $CoSO_4$ or 0.05 M $Ce(CH_3COO)_3$ solution, the electrode surface becomes locally alkaline (Eq. 12 and 13) due to ORR during pretreatments at the potential at which the electrode was held, which is within the range of the measured open-circuit potential of AA2024-T3.[73]

This local alkalinity leads to the formation of insoluble oxides, hydroxides, or oxi-hydroxides, e.g.

$$Co^{2+} + 2\ OH^- \rightarrow Co(OH)_{2(s)} \quad (pK_{SP} = 14.23) \qquad [12]$$

$$Ce^{3+} + 3\ OH^- \rightarrow Ce(OH)_{3(s)} \quad (pK_{SP} = 26.15) \qquad [13]$$

The negative logarithms of solubilities (pK_{SP}) are shown in parentheses.[82] The speciation diagrams for Ce^{3+} and Co^{2+} are shown in Fig. 12 and 13. As shown in Fig. 12, insoluble $Co(OH)_{2(s)}$ is the dominant species under alkaline conditions (pH > 7). Thus, alkaline pH is required for the homogeneous precipitation of $Co(OH)_2$. The rate of precipitation may be faster as the pH increases, since the concentration of one of the reactants (OH^-) increases. According to the speciation diagram of the Ce^{3+}-water system shown in Fig. 13, the insoluble $Ce(OH)_{3(s)}$ is predominant under alkaline conditions (pH > 7.2). However, in case of the Ce^{3+} pretreatment, the oxidation of Ce from a +3 oxidation state to a +4 oxidation state is also possible. It was shown that the oxidation occurs regardless of the pathway of ORR (two- or four-electron process).[46] If the ORR takes place via the overall four-electron process, the dissolved oxygen oxidizes the Ce^{3+} directly[46]

$$4Ce^{3+} + O_2 + 4\ OH^- + 2H_2O \rightarrow 4Ce(OH)_2^{2+} \qquad [14]$$

In case of the two-electron ORR pathway, the hydrogen peroxide oxidizes the Ce^{3+}[46]

$$2Ce^{3+} + 2\ OH^- + H_2O_2 \rightarrow 2Ce(OH)_2^{2+} \qquad [15]$$

The Ce^{4+} is highly insoluble under alkaline conditions as shown in Fig. 14. Therefore, the $Ce(OH)_2^{2+}$ complex likely reacts with the OH^- ions present to form a highly insoluble ($pK_{SPa} = 8.164$, calculated from thermodynamic data[78] assuming the following reaction: $CeO_2 + 4H^+ \rightarrow Ce^{4+} + 2H_2O$) CeO_2 precipitate[46]

$$Ce(OH)_2^{2+} + 2\ OH^- \rightarrow CeO_2 + 2H_2O \qquad [16]$$

This precipitated film partially blocks the surface to oxygen reduction. It was suggested[48] that Ce(III) film formation on Cu is irreversible, that is, once the inhibitor reacts with the surface, it remains there despite removing the inhibiting species from the solution, and immersing the treated electrode into an inhibitor-free solution. This theory assumes that the pH does not shift significantly in the acidic direction, which would cause the chemical dissolution of the precipitate. Our tests conducted at various pH values suggest that the slightly alkaline environment (pH 7 and 8.2) causes the most significant reduction of the cathodic current density associated with ORR. Under more alkaline conditions, only a moderate reduction in

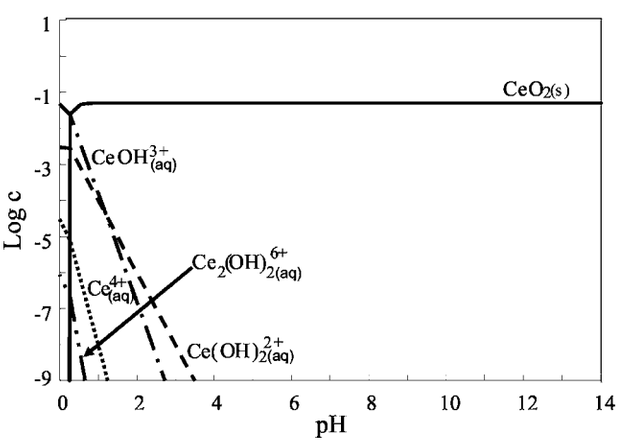

Figure 14. Logarithm of concentrations of chemical species present in Ce^{4+}-water system. The bulk concentration of Ce^{4+} ions is 0.05 M.

ORR was observed. This behavior is not supported by the speciation diagram of Ce^{3+} (Fig. 13) or Ce^{4+} (Fig. 14) ions. This may be attributed to the formation of a coarser Ce deposit as the pH is raised, which results in less blocking of the O_2 transport. In support of this theory the morphology of the Ce deposit was shown to be highly dependent on the local pH at the surface, and larger particles and crystalline Ce precipitate forms at higher pH values on AA7075.[64]

According to Fig. 5a, the reduction in cathodic current density was not as high for potentiodynamic polarization tests at rotation rates higher than 500 rpm as for the scans conducted below 500 rpm. However, moderate reduction of the ORR was still observed at even fairly high rotation rates ($\geqslant$2000 rpm). These results suggest the possibility that the shear stress induced by high flow rates can strip the cerium hydroxide/oxide film off the Cu surface. Interestingly, when the rotation starts at a slow rotation rate in a chronoamperometric test, the cathodic current density values are lower than the corresponding i_{total} values determined from the potentiodynamic curves suggesting that the film stays intact even if the rotation rate is raised to a fairly high value later (Fig. 6). It was found that the Ce pretreatment is most effective in reducing ORR on Cu under moderately alkaline conditions (in a pH range of 7–8.2), in a potential range of -0.65 to -0.95 V_{SCE}. The largest effect was found at low rotation rates and in potentiostatic tests that started at low rotation rates (Fig. 6), indicating that the Ce film might perform adequately under stagnant conditions. Ce^{3+} has been reported to reduce the cathodic kinetics. However, i_{dl} is not completely independent of the rotation rate.[48] Similar results were found in this investigation.

As indicated in the Results section, pretreatment in $CoSO_4$ solution reduced the cathodic current density significantly at potentials more noble than -0.85 V_{SCE} when tested in pH 9.5 (Fig. 5d). The effect was less pronounced at lower pH values (Fig. 5c).

The speciation diagram of the Co^{2+}-water system (Fig. 12) suggests that the insoluble $Co(OH)_2$ is the dominant species under alkaline conditions (pH $>$ 7) indicating that the film precipitated on the Cu surface during the pretreatment is mainly composed of $Co(OH)_2$. According to the potential-pH diagram of the Co^{2+}-water system, at potentials below -0.71 V_{SCE} (at pH 9.5), the $Co(OH)_2$ is reduced to Co(0)

$$Co(OH)_2 + 2H^+ + 2e^- \rightarrow Co + 2H_2O \qquad [17]$$

The HER occurs slightly below this potential [-0.80 V_{SCE} (at pH 9.5)]. The precipitated $Co(OH)_2$ will therefore be reduced to Co(0), thus the large increase in cathodic current density below -0.8 V_{SCE} (Fig. 5c,d and 6) can be attributed to $Co(OH)_2$ reduction and HER reactions. The hydroxide precipitate is apparently stable, as in the test solution of pH 9.5, during the first 0.4 V of the cathodic scan, which explains the very small current measured.

It has been suggested that Co(III) might provide even better protection over a larger range of pH[63] as part of a conversion coating system than Co(II). However, the oxidation of Co(II) to Co(III) occurs only at elevated temperatures or in the presence of catalysts with the aid of strong oxidizers (e.g., hydrogen peroxide) in solutions containing cobalt(II)ammines.[63,83] Therefore, it is unlikely that the film contains Co(III). During pretreatment, the pH in the vicinity of the Cu surface increases as a result of ORR in the unbuffered solution. This pH shift promotes the precipitation of $Co(OH)_2$.

The MoO_4^{2-} ions can be electrochemically reduced to Mo(IV) on the surface of copper to form chemically insoluble MoO_2 (pK_{SP} = 13.39[82]) during pretreatment at the OCP of AA2024-T3[73] provided that the pH is not too alkaline (Eq. 3).

This reaction (Eq. 3) occurs at approximately -0.65 V_{SCE} during pretreatment (pH 8.5). The treatment potentials were -0.50 V_{SCE} and -0.70 V_{SCE}. However, local changes of the pH on the surface to pH values as high as 9 or 10 can cause potential shifts allowing the formation of MoO_2 at the treatment potential of -0.50 V_{SCE}. Alternatively, MoO_4^{2-} could be chemisorbed during the pretreatment.

In our case, it is likely that the film contains chemisorbed MoO_4^{2-}, because the pretreatment was conducted in moderately alkaline solution (pH $\sim$ 8.5). MoO_2 can form during the cathodic scan. However, the pretreatment at lower potentials in this solution can result in the formation of MoO_2 as well.[73]

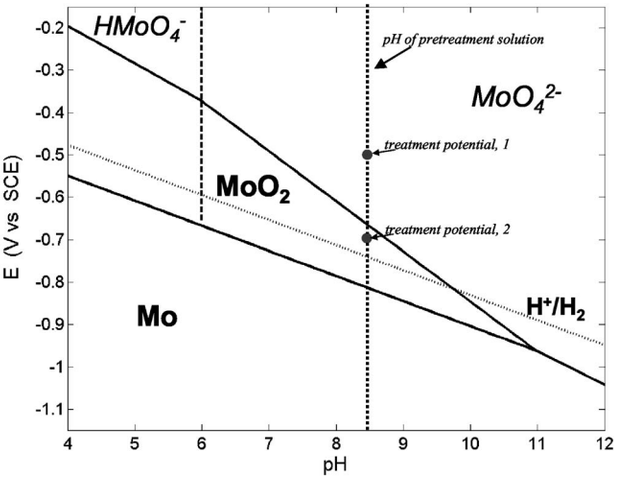

Figure 15. Pourbaix diagram of the molybdenum-water system at 25°C. The concentration of dissolved species was assumed to be 0.1 M.[73]

The polarization curves on Cu after Mo pretreatment show a valley at around -0.81 V_{SCE} when tested in solution of pH 8.2 (Fig. 4a and b). This feature seems to be independent of the pretreatment potential (Fig. 4a and b). After the valley, the current density increases with further cathodic polarization. This feature was analyzed using the potential-pH diagram of the molybdenum water system shown in Fig. 15.[73]

The experimental potential and pH values are indicated in Fig. 15. The analysis of the diagram shows that at around -0.67 V_{SCE}, the reaction of Eq. 3 occurs in the forward direction, and MoO_2 forms by electrochemical reduction on the surface, which has fairly low solubility (pK_{SP} = 13.39[82]). The Nernst potential of this reaction depends on both the solution pH and the molybdate ion concentration according to Eq. 4.[73]

Local pH increase (shift to the alkaline direction) upon further cathodic polarization causes the oxidative dissolution of MoO_2, depending on whether the pH increases faster than the potential drops. This potential and pH dependent dissolution/oxidation process occurs above pH 9. This reaction or MoO_2 reduction to Mo at fixed pH and fast potential drop might be responsible for the increase in current density as the potential becomes more negative. Enough cathodic polarization can allow the buffer capacity[84] to be surpassed, and no more MoO_2 is formed after passing a critical pH (which will depend on the exact potential and pH).

In combination, these inhibitors could inhibit ORR on Cu-rich sites on an Al alloy over a pertinent pH-potential range for corrosion. Ce and Mo might act best at pH 8-9 while Co could operate at pH 9-11. Inhibition could be effective from -0.6 to -1.0 V_{SCE} relevant to alloy 2024-T3.

Conclusions

A four-electron ORR mechanism was found to take place on Cu and on Au in natural aerated borate solution at potential values ranging from -0.75 to -1.05 V_{SCE}. In general, i_{dl} values on Au are slightly larger than on Cu for corresponding sets of conditions possibly due to Cu oxides.

In all cases preceded by inhibitor pretreatments, a decrease in the cathodic ORR kinetics is observed to different degrees over the potential range from -0.6 to -1.0 V_{SCE}. The rotation rate dependence on Cu after Co and Ce treatments is consistent with film precipitation on a homogeneous electrode. The cathodic polarization

scans after Mo treatment assumes an unusual shape interpreted as the formation of MoO_2 followed by pH driven oxidative dissolution of MoO_2 to MoO_4^{2-} or potential driven reduction of this inhibiting oxide (e.g., MoO_2 to Mo).

Co reduced the cathodic kinetics the most when tested in a solution of pH 9.5 consistent with low solubility of $Co(OH)_2$ at high pH; Ce pretreatment gives the best result at pH 8.2 and pH 7. The best Ce results were obtained during the chronoamperometric test when the electrode was held at -0.95 V_{SCE}, following a cathodic scan at 100 rpm. In contrast, Mo was most effective when tested in pH 8.2 solution and became ineffective at pH 11, which is consistent with the limited range of stability of MoO_2.

Acknowledgments

A Multi-University Research Initiative (grant no. F49602-01-1-0352) entitled *"The Development of an Environmentally Compliant Multifunctional Coating for Aerospace Applications using Molecular and Nano-Engineering Methods"* supported this work under the direction of Dr. Jennifer Gresham at AFOSR.

The University of Virginia assisted in meeting the publication costs of this article.

References

1. G. S. Chen, M. Gao, and P. P. Wei, *Corrosion (Houston)*, **52**, 8 (1996).
2. R. G. Buchheit, R. P. Grant, P. F. Hlava, B. Mckenzie, and G. L. Zender, *J. Electrochem. Soc.*, **144**, 2621 (1997).
3. J. R. Scully, T. O. Knight, R. G. Buchheit, and D. E. Peebles, *Corros. Sci.*, **35**, 185 (1993).
4. M. J. Pryor and D. S. Keir, *J. Electrochem. Soc.*, **102**, 241C (1955).
5. R. G. Buchheit, *J. Electrochem. Soc.*, **142**, 3994 (1995).
6. G. O. Ilevbare, J. R. Scully, J. Yuan, and R. G. Kelly, *Corrosion (Houston)*, **56**, 227 (2000).
7. O. Schneider, G. O. Ilevbare, J. R. Scully, and R. G. Kelly, *Electrochem. Solid-State Lett.*, **4**, B35 (2001).
8. *Aluminum, Properties and Physical Metallurgy*, J. E. Hatch, Editor, ASM International, Materials Park, OH (1984).
9. M. B. Vukmirovic, N. Vasiljevic, N. Dimitrov, and K. Sieradzki, *J. Electrochem. Soc.*, **150**, B10 (2003).
10. S. Cere, S. R. de Sanchez, and D. J. Schiffrin, *J. Electroanal. Chem.*, **386**, 165 (1995).
11. M. V. Vazquez, S. R. de Sanchez, E. J. Calvo, and D. J. Schiffrin, *J. Electroanal. Chem.*, **374**, 189 (1994).
12. M. B. Vukmirovic, N. Dimitrov, and K. Sieradzki, *J. Electrochem. Soc.*, **149**, B428 (2002).
13. N. Dimitrov, J. A. Mann, and K. Sieradzki, *J. Electrochem. Soc.*, **146**, 98 (1999).
14. M. A. Jakab, F. Presuel-Moreno, and J. R. Scully, *Corrosion (Houston)*, **61**, 246 (2005).
15. G. O. Ilevbare and J. R. Scully, *J. Electrochem. Soc.*, **148**, B196 (2001).
16. G. O Ilevbare and J. R. Scully, *Corrosion (Houston)*, **57**, 134 (2001).
17. W. Paatsch, *Metalloberflache*, **45**, 369 (1991).
18. M. Kending and R. Buchheit, CORROSION/2000, NACE, Houston, pp. 1–31 (2000).
19. C. M. Reddy, Q. S. Yu, C. E. Moffitt, D. M. Wieliczka, R. Johnson, J. E. Deffeyes, and H. K Yasuda, *Corrosion (Houston)*, **56**, 819 (2000).
20. J. Zahavi, *Corrosion Reviews*, **15**, 341 (1997).
21. B. A. Shaw, G. D. Davis, T. L. Fritz, and K. A. Olver, *J. Electrochem. Soc.*, **137**, 359 (1990).
22. B. R. W. Hinton, D. R. Arnott, and N. E. Ryan, *Met. Forum*, **7**, 211 (1984).
23. M. W. Kending and R. G. Buchheit, *Corrosion (Houston)*, **59**, 379 (2003).
24. L. Xia, E. Akiyama, G. Frankel, and R. McCreery, *J. Electrochem. Soc.*, **147**, 2556 (2000).
25. C. S. Jeffcoate, H. S. Isaacs, A. J. Aldykiewicz, Jr., and M. P. Ryan, *J. Electrochem. Soc.*, **147**, 540 (2000).
26. L. Xia and R. L. McCreery, *J. Electrochem. Soc.*, **145**, 3083 (1998).
27. M. Gao, N. Unlu, M. Jakab, J. Scully, and G. J. Shiflet, *Tri-Services Corrosion Conference*, San Antonio, TX, p. 1323 (2002).
28. M. E. Goldman, N. Ünlü, J. Shiflet, and J. R. Scully, *Electrochem. Solid-State Lett.*, **8**, B1 (2005).
29. V. A. Kumari, K. Sreevalsan, and S. M. Shibli, *Corros. Prev. Control*, **48**, 83 (2001)
30. R. G. Buchheit, S. B. Mmidipally, P. Schmutz, and H. Guan, *Corrosion (Houston)*, **58**, 3 (2002).
31. M. Bethancourt, F. Botana, J. Calvino, M. Marcos, and M. Rodriguez-Chacon, *Corros. Sci.*, **40**, 1803 (1998).
32. W. C. Moshier and G. D. Davis, *Corrosion (Houston)*, **46**, 43 (1990).
33. K. C. Emregül and A. A. Aksüt, *Corros. Sci.*, **45**, 2415 (2003).
34. J. Augustynski, in *Passivity of Metals*, p. 989, R. P. Frankenthal and J. Kruger, Editors, The Electrochemical Society Proceedings Series, Pennington, NJ (1978).
35. F. Mansfeld, in *H.H. Uhlig Memorial Symposium*, PV 94-26, p. 65, F. Mansfeld, A. Asphahani, H. Bohni, and R. Latanision, Editors, The Electrochemical Society Proceedings Series, Pennington, NJ (1995).
36. F. Mansfeld and Y. Wang, *Br. Corros. J., London*, **29**, 194 (1994).
37. A. W. Armour and D. R. Robitaille, *J. Chem. Technol. Biotechnol.*, **29**, 619 (1979).
38. J. N. Wanklyn, *Corros. Sci.*, **21**, 211 (1981).
39. G. D. Wilcox and D. R. Gabe, *Br. Corros. J., London*, **22**, 254 (1987).
40. G. D. Wilcox and D. R. Gabe, *Corros. Sci.*, **28**, 577 (1988).
41. B. Mosayebi, M. Kazemeini, A. Badakhshan, and A. Safekordi, *Anti-Corros. Methods Mater.*, **49**, 426 (2002).
42. R. Arnot, B. R. W. Hinton, and N. E. Ryan, *Corrosion (Houston)*, **45**, 12 (1989).
43. K. Aramaki, *Corros. Sci.*, **43**, 2201 (2001).
44. K. Aramaki, *Corros. Sci.*, **44**, 1361 (2002).
45. K. Aramaki, *Corros. Sci.*, **44**, 871 (2002).
46. A. J. Aldykiewicz, Jr., A. J. Davenport, and H. S. Isaacs, *J. Electrochem. Soc.*, **143**, 147 (1996).
47. A. J. Aldykiewicz, Jr., H. S. Isaacs, and A. J. Davenport, *J. Electrochem. Soc.*, **142**, 3342 (1995).
48. M. Kending and S. Jeanjaquet, *J. Electrochem. Soc.*, **149**, B47 (2002).
49. P. Traverso, R. Spiniello, and L. Monaco, *Surf. Interface Anal.*, **34**, 185 (2002).
50. A. S. Hamdy, A. M. Beccaria, and P. Traverso, *Surf. Interface Anal.*, **34**, 171 (2002).
51. B. Y. Johnson, J. Edington, and M. J. O'Keefe, *Mater. Sci. Eng., A*, **361**, 225 (2003).
52. L. Domingues, C. Oliveira, J. C. S. Fernandes, M. G. S. Ferreira, and T. E. Fonseca, *Key Eng. Mater.*, **230-232**, 392 (2002).
53. F. Mansfeld, S. Lin, S. Kim, and H. Shih, *Corrosion (Houston)*, **45**, 615 (1989).
54. C. M. Rangel, P. P. da Luz, and T. I. Paiva, *Key Eng. Mater.*, **230-232**, 68 (2002).
55. M. Forsyth et al. *Corros. Sci.*, **44**, 2651 (2002).
56. M. A. Arenas, A. Conde, and J. J. de Damborenea, *Corros. Sci.*, **44**, 511 (2002).
57. W. Zhang, J. Li, C. Gu, and D. Shen, *Corrosion Science and Protection Technology*, **13**, 128 (2001).
58. S. Powell, *Surf. Eng.*, **16**, 169 (2000).
59. M. A. Arenas et al., *Corros. Sci.*, **43**, 157 (2001).
60. A. Aballe et al., *J. Alloys Compd.*, **323**, 855 (2001).
61. A. Aballe et al., *Mater. Corros.*, **52**, 344 (2001).
62. M. Kabasakaloglu, H. Aydin, and M. L. Aksu, *Mater. Corros.*, **48**, 744 (1997).
63. M. P. Schriever, The Boeing Company, U.S. Pat: 5,298,092 (1994); 5,378,293 (1995); 5,415,687 (1995); 5,472,524 (1995); 5,487,949 (1996); 5,411,606 (1995); 5,551,994 (1996); 5,873,953 (1999); 6,432,225 (2002).
64. B. R. Hinton, *New Approaches to Corrosion Inhibition with Rare Earth Metal Alloys, Corrosion/89*, Paper 170 (1989).
65. S. Virtanen, M. B. Ives, G. I. Sproule, P. Schmuki, and M. J. Graham, *Corros. Sci.*, **39**, 1897 (1997).
66. Y. C. Lu and M. B. Ives, *Corros. Sci.*, **37**, 145 (1995).
67. M. Bethancourt, F. Botana, J. Calvino, and M. Marcos, *Appl. Surf. Sci.*, **189**, 162 (2002).
68. V. N. Vigdorovich, V. M. Glazov, and N. N. Glagoleva, *Izv. Vyssh. Uchebn. Zaved., Tsvetn. Metall.*, **3**, 143 (1960).
69. P. Rontgen and W. Koch, *Z. Metallkd.*, **25**, 182 (1933).
70. E. L. Principe, B. A. Shaw, and G. D. Davis, *Corrosion (Houston)*, **59**, 295 (2003).
71. P. H. Chong, H. C. Man, and T. M. Yue, *Surf. Coat. Technol.*, **145**, 51 (2001).
72. X. Zhang et al., *Corros. Sci.*, **43**, 85 (2001).
73. M. Pourbaix, *Atlas of Electrochemical Equilibria in Aqueous Solutions*, translated by J. A. Franklin, NACE, Houston (1974).
74. V. G. Levich, *Physicochemical Hydrodynamics*, Prentice Hall, Englewood Cliffs, NJ (1962).
75. J. P Hoare, *The Electrochemistry of Oxygen*, John Wiley & Sons, New York (1968).
76. E. Gileadi, *Electrode Kinetics for Chemists, Chemical Engineers and Materials Scientists*, John Wiley-VCH, New York (1993).
77. K. E. Gubbins and R. D. Walker, *J. Electrochem. Soc.*, **112**, 469 (1965).
78. *CRC Handbook of Chemistry and Physics*, 79th ed., D. R. Lide, Editor, CRC Press LCC, Boca Raton, FL (1999).
79. X. Zhang S. Lo Russo, S. Zandolin, A. Miotello, E. Cattaruzza, P. L. Bonora, and L. Benedetti, *Corros. Sci.*, **43**, 85 (2001).
80. S. Strbac, N. A. Anastasijevic, and R. R. Adzic, *J. Electroanal. Chem.*, **323**, 179 (1992).
81. H. Kaesche, *Metallic Corrosion: Principles of Physical Chemistry and Current Problems*, translated by R. A. Rapp, NACE, Houston, TX (1985).
82. I. Puigdomenech, MEDUSA/HYDRA Chemical Equilibrium Software, Dept. of Inorganic Chemistry, Royal Institute of Technology, Stockholm, Sweden (2002).
83. N. N. Greenwood and A. Earnshaw, *Chemistry of the Elements*, 2nd ed., Butterworth-Heinemann, Boston (1998).
84. D. A. Skoog, D. M. West, and F. J. Holler, *Fundamentals of Analytical Chemistry*, 7th ed., Saunders College, Fort Worth, TX (1996).